Vol 18 No 6, June 2009
1674-1056/2009/18(06)/2432-09

Chinese Physics B

© 2009 Chin. Phys. Soc.
and IOP Publishing Ltd

The stability margin on EAST tokamak*

Qian Jin-Ping(钱金平)[a)†], Wan Bao-Nian(万宝年)[a)], Shen Biao(沈 彪)[a)], M.L. Walker[b)], D.A. Humphreys[b)], and Xiao Bing-Jia(肖炳甲)[a)]

[a)] *Institute of Plasma Physics, Chinese Academy of Sciences, Hefei* 230031, *China*
[b)] *General Atomics, San Diego, California, USA*

(Received 7 June 2008; revised manuscript received 23 October 2008)

The experimental advanced superconducting tokamak (EAST) is the first full superconducting tokamak with a D-shaped cross-sectional plasma presently in operation. Its poloidal coils are relatively far from the plasma due to the necessary thermal isolation from the superconducting magnets, which leads to relatively weaker coupling between plasma and poloidal field. This may cause more difficulties in controlling the vertical instability by using the poloidal coils. The measured growth rates of vertical stability are compared with theoretical calculations, based on a rigid plasma model. Poloidal beta and internal inductance are varied to investigate their effects on the stability margin by changing the values of parameters α_n and γ_n(Howl *et al* 1992 *Phys. Fluids* B **4** 1724), with plasma shape fixed to be a configuration with $k = 1.9$ and $\delta = 0.5$. A number of ways of studying the stability margin are investigated. Among them, changing the values of parameters κ and l_i is shown to be the most effective way to increase the stability margin. Finally, a guideline of stability margin $M_s(\kappa, l_i, A)$ to a new discharge scenario showing whether plasmas can be stabilized is also presented in this paper.

Keywords: vertical instability, growth rate, stability margin
PACC: 5255, 5235P, 5255G

1. Introduction

Tokamak plasmas with elongated cross sections tend to be unstable to an axisymmetric mode, leading to a vertical displacement of the plasma. During the vertical motion, the plasma current decays, owing to its interaction with the vacuum vessel. The vessel experiences a vertical reaction force as it attempts to slow down the plasma motion.[1−5] The experimental advanced superconducting tokamak (EAST) is the first full superconducting tokamak (superconducting poloidal and toroidal coils) with a D-shaped cross-sectional plasma presently in operation. In the first experimental campaign, we successfully obtained reliable plasma initiation, current ramp up and RZIP control (RZ stands for R and Z positions, and IP for plasma current). The principal goal of the second operation campaign was to obtain a shaped diverted plasma by using optimized plasma control algorithm. Limiter, single null and double null diverted configurations were produced in this campaign.[6]

Some of EAST discharges were disrupted after failure of feedback control of the vertical instability. One main reason was that the poloidal coils were relatively far from the plasma due to the necessary thermal isolation from the superconducting magnets,[7] which led to relatively weaker coupling between plasma and poloidal field (see in Fig.1). Under this circumstance, a better passive stabilization will serve as the control field provided by the active control coils.

The present work is to investigate the stability margin of EAST device with equilibrium configuration by using the EFIT code[8] and to further guide a new discharge scenario, and so we can obtain valuable information on whether the plasma can be vertically stabilized. The remainder of the present paper is organized as follows. In Section 2, we describe the passive structure of the EAST tokamak and then determine the stability boundary (critical decay index). The plasma response model, measurement results of the growth rate of vertical stability and the comparison between calculations and measurements are presented in Section 3. The primary results and the compromising parametric study are described in Section 4. Summary and discussion are given in Section 5.

*Project supported by National Natural Science Foundation of China (Grant Nos 10725523 and 10835009).
†E-mail: jpqian@ipp.ac.cn

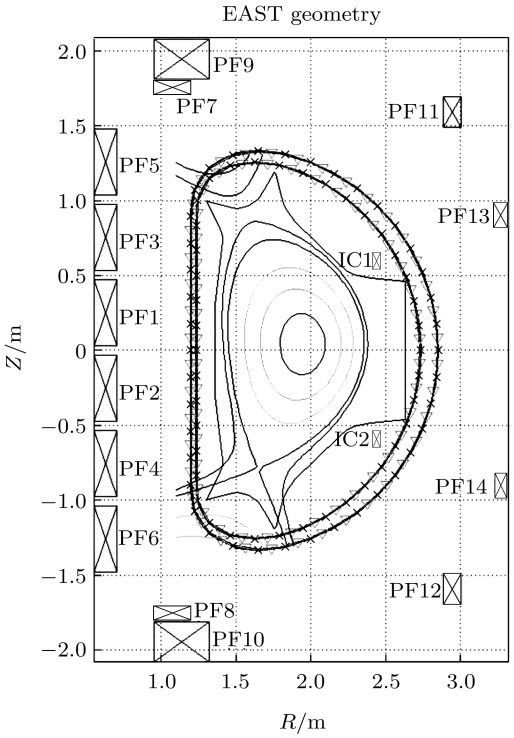


Fig.1. Cross section of the EAST device, showing the locations of all the 14 poloidal field (PF) coils and inner control (IC) coils (single null plasma configuration) and the double vacuum vessel that is composed of 80 segments.

2. EAST tokamak

The EAST is designed to be up-down symmetric, (see in Fig.1) and its structural parameters are $R = 1.8$ m, $a = 0.45$ m, $B_\phi = 3.5$ T, and $I_p = 1$ MA for highly elongated plasma with $\kappa = 1.9$. It can be operated in very flexible plasma shapes, for example, in double null or single null configurations with elongation $\kappa = 1$–1.9 and triangularity δ being up to 0.65.

The vacuum vessel is a continuously welded structure with low toroidal resistance ($\sim$76 $\mu\Omega$) and a D-shaped cross section. To be fully capable of producing different configurations, the EAST is equipped with a set of 12 independently powered poloidal shaping coils and a pair of water-cooled fast copper coils inside the vacuum vessel (see IC1 and IC2 in Fig.1). The fast coils are powered by a fast power supply and used to stabilize plasmas with high vertical growth rates.

2.1. Passive structure

The vacuum vessel is made of 8 mm thick stainless steel plates. Port holes in the vessel make the electromagnetic modeling difficult. Instead of a complicated three-dimensional representation, a toroidally symmetric model determining spatial distribution of the effective resistivity is chosen. The vacuum vessel is composed of 80 segments (40 segments for the inner vessel and 40 segments for the outer vessel as shown in Fig.1). Figures 2, 3 and 4 summarize the features of the vessel for the version of passive structure.

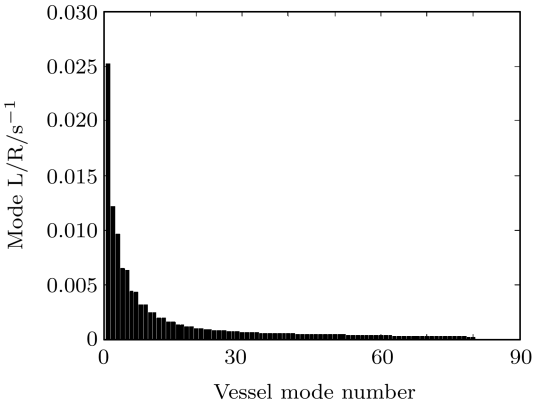
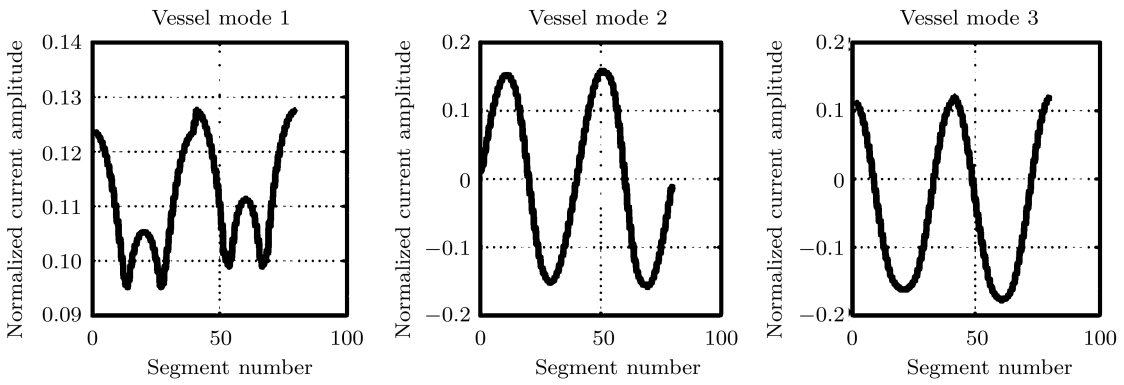


Fig.2. L/R time constant of vacuum vessel eddy current mode versus vessel mode number.



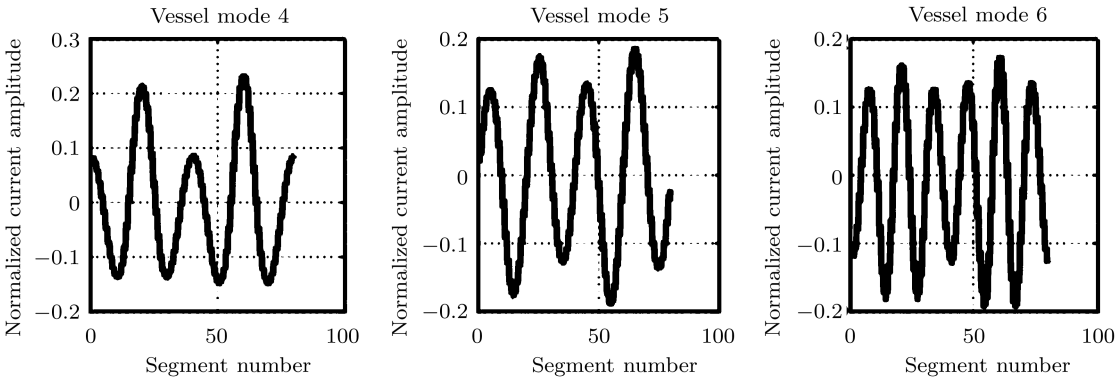


Fig.3. Normalized current distribution in the vessel wall for the first 6 vessel eigenmodes, where x axis represents segment number of the vacuum vessel and y axis refers to normalized current amplitude.

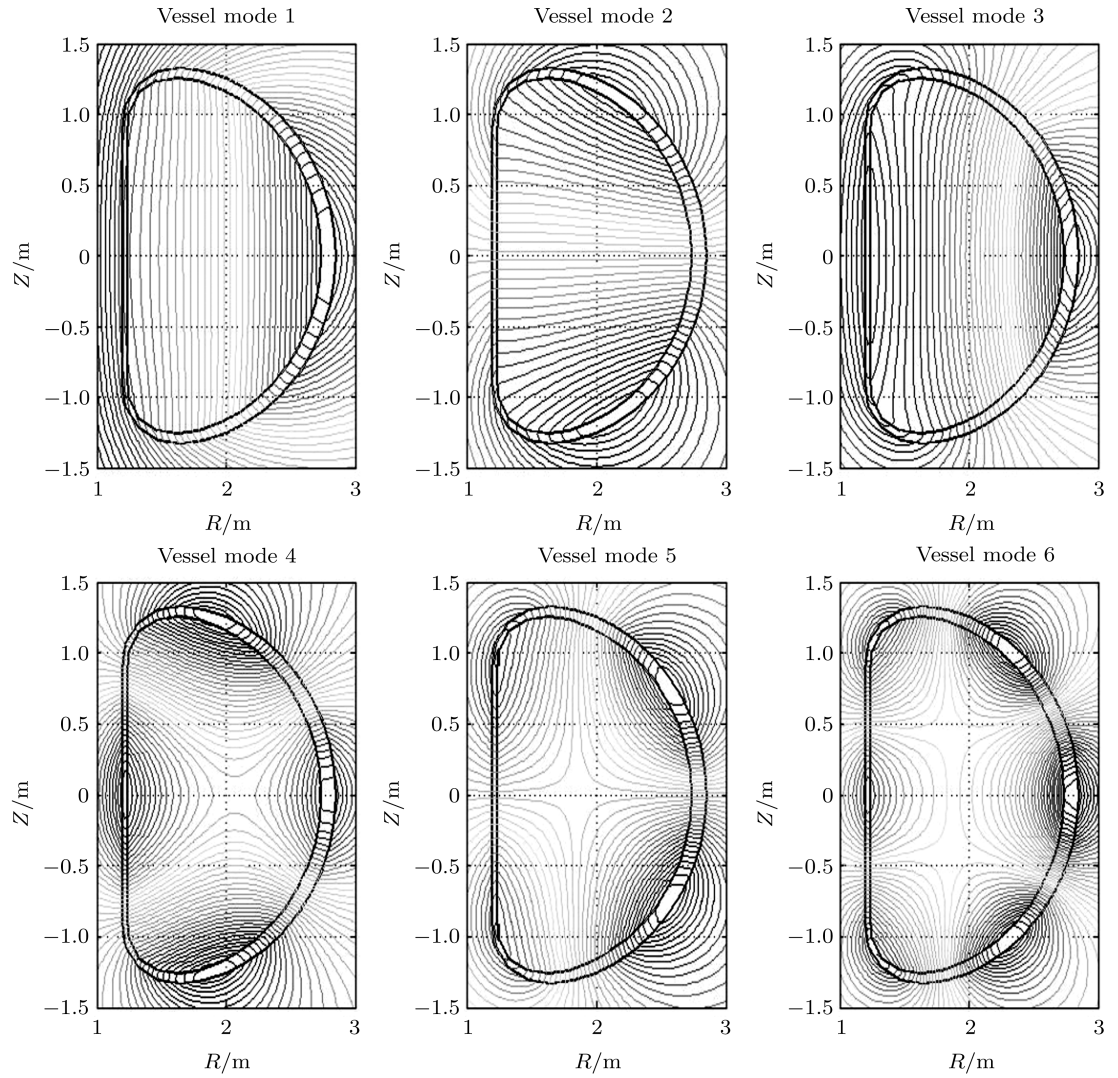


Fig.4. Flux contours associated with the first six eigenmodes of the vessel.

Figure 2 shows eigenmodes of the vacuum vessel, which are arranged in decreasing order of L/R time. The second mode with decay time $\tau_s = 13$ ms dominates in terms of passive stabilization. Details of this analysis method are well documented in Refs.[9]–[11]. As shown in Fig.3 for the first six eigenmodes, we see that the vessel eigenmodes 2 and 5 are up-down asymmetric modes while the other eigenmodes are up-down symmetric.

Thus the vertical plasma position stabilization is chiefly due to modes 2 and 5. The flux distributions corresponding to eigenmodes (1–6) are presented in Fig.4, showing the radial field components associated with modes 2 and 5.

2.2. Critical index

As is known, the growth rate of the vertical instability of an elongated plasma depends on the destabilizing curvature of the external field (quadrupole field) and on the stabilization function of the passive structure surrounding the plasma. The passive structure circuit equation can be written as

$$M_{\rm ss}\dot{I}_{\rm s} + R_{\rm s}I_{\rm s} + \frac{\partial\psi_{\rm sp}}{\partial z}\frac{\partial z}{\partial I_{\rm s}}\dot{I}_{\rm s} = V_{\rm s}, \tag{1}$$

where M and R are the mutual inductance and resistance matrix of the structure, V is the voltage, the subscripts s and p refer to the structure (including poloidal coils and passive structure) and the plasma respectively. Solving the force balance equation and defining the decay index n as[12]

$$n \equiv -\frac{1}{I_{\rm p}B_{z0}}\int RJ_\phi\left(\frac{\partial B_R}{\partial z}\right){\rm d}R{\rm d}z \tag{2}$$

at the point of ideal instability, allowing growth rate $\gamma \to \infty$ as $n \to n_c$, the critical index n_c is given by[13]

$$n_c = \frac{1}{2\pi B_{z0}I_{\rm p0}}{\rm Tr}\left\{M_{\rm ss}^{-1}\left(\frac{\partial M_{\rm sp}}{\partial z}\boldsymbol{I}_{\rm p}\right)\left(\boldsymbol{I}_{\rm p}^T\frac{\partial M_{\rm ps}}{\partial z}\right)\right\}, \tag{3}$$

where Tr denotes the matrix trace, $\boldsymbol{I}_{\rm p}$ is the vector of plasma current element on the grid. Ignoring the plasma current distribution, expression (3) can be simply expressed as

$$n_c' = \frac{2R_0}{\mu_0\Gamma}{\rm Tr}\left\{M_{\rm ss}^{-1}\frac{\partial M_{\rm sp}}{\partial z}\frac{\partial M_{\rm ps}}{\partial z}\right\}, \tag{4}$$

where $\Gamma \equiv \ln(8R_0/a) + \Lambda - 3/2$ is the Shafranov vertical field coefficient with $\Lambda \equiv \beta_p + l_i/2$.

Figure 5 shows critical decay index (n_c') plotted as a function of Λ, ignoring the plasma current distribution. Note that this curve is for $R_0 = 1.85$ m, and $a = 0.45$ m. If we treat Λ over a range of 0.8–2.5 as typical parameters of EAST discharge, n_c' will drop down from 2.2 to 1.4. For any EAST discharge $n/n_c > 1$, the plasma will move on an Alfven time scale after a vertical position perturbation because the surrounding conducting structures no longer slow the instability to their resistive time scale.

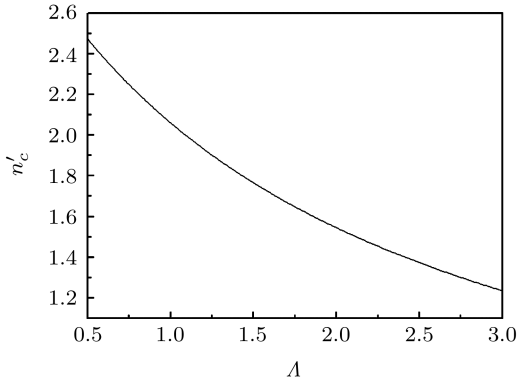


Fig.5. Critical decay index (equation 4) vs. Shafranov Λ.

3. Open loop growth rates

3.1. Plasma response model

The system of plasma, poloidal field (PF) coils and passive structure can be described by using circuit equations derived from Faraday's law, and radial and vertical force balance relations for a presented plasma equilibrium. The linearized model equations for the currents in PF coils and vessel and the plasma current are respectively given as follows:

$$\begin{aligned} &M_{cc}^*\dot{I}_c + R_cI_c + M_{cv}^*\dot{I}_v + M_{cp}^*\dot{I}_p = V_c,\\ &M_{vv}^*\dot{I}_v + R_vI_v + M_{vc}^*\dot{I}_c + M_{vp}^*\dot{I}_p = 0,\\ &M_{pp}^*\dot{I}_p + R_pI_p + M_{pc}^*\dot{I}_c + M_{pv}^*\dot{I}_v = V_{\rm no}, \end{aligned} \tag{5}$$

where I, V and R represent current, voltage and resistance respectively; the subscripts c, v and p represent PF coil, vessel and plasma respectively; $V_{\rm no}$ is the effective voltage used to drive plasma current by non-inductive sources; $M_{ab}^* = M_{ab} + X_{ab}$ is plasma modified mutual inductance, where $a, b \in \{c, v, p\}$, with M_{ab} being the usual conductor-to-conductor mutual inductance and X_{ab} being the plasma motion-mediated inductance. The plasma response matrix X_{ab}, representing changes in flux due to plasma motion, is a function of equilibrium current distribution and vacuum field. As an example we consider $X_{ab} = X_{ab}(r_c, z_c, I_p)$ by using the rigid model. The dynamic equation (5) can be written as

$$M\dot{I} + RI = V$$

with $I = [I_c^T, I_v^T, I_p]^T$, $V = [V_c^T, 0, V_{\rm no}]^T$.

The conductors-only portion of the matrix M given by

$$\begin{bmatrix} M_{cc}+\left(\dfrac{\partial M_{cp}}{\partial z_c}\dfrac{\partial z_c}{\partial I_c}+\dfrac{\partial M_{cp}}{\partial r_c}\dfrac{\partial r_c}{\partial I_c}\right)I_{p,eq} & M_{cv}+\left(\dfrac{\partial M_{cp}}{\partial z_c}\dfrac{\partial z_c}{\partial I_v}+\dfrac{\partial M_{cp}}{\partial r_c}\dfrac{\partial r_c}{\partial I_v}\right)I_{p,eq} \\ M_{vc}+\left(\dfrac{\partial M_{vp}}{\partial z_c}\dfrac{\partial z_c}{\partial I_c}+\dfrac{\partial M_{vp}}{\partial r_c}\dfrac{\partial r_c}{\partial I_c}\right)I_{p,eq} & M_{vv}+\left(\dfrac{\partial M_{vp}}{\partial z_c}\dfrac{\partial z_c}{\partial I_v}+\dfrac{\partial M_{vp}}{\partial r_c}\dfrac{\partial r_c}{\partial I_v}\right)I_{p,eq} \end{bmatrix}$$

must be symmetric and R is a diagonal matrix (all its elements are positive or zero). Therefore the eigenvalues cannot be imaginary. Note that those undefined notations follow those in Ref.[14].

3.2. Comparison between model and experiment

The vertical instability growth rates have been measured experimentally in the EAST for several shots. The measurement is performed by opening the position feedback control loops during the quasi-stationary phase and observing the growth of the vertical displacement via the magnetic diagnostics. The proportional integral derivative (PID) feedback gain was set to be zero by using a pre-programmed switch. A typical example of an unstable vertical displacement with the feedback cut is shown in Fig.6. The experimental values of growth rate are evaluated by fitting the time evolution

$$z(t) = z_0 + \delta z \mathrm{e}^{\int_{t_0}^{t}\gamma(\tau)\mathrm{d}\tau}.$$

The initial time, t_0, is chosen to be the moment after feedback control loops cut, and the final time, t, is selected to be the moment before significant non-linear effects occur. Otherwise the system will enter non-linear regimes, i.e. the two terms $\mathrm{d}\beta_p/\mathrm{d}t$ and $\mathrm{d}l_i/\mathrm{d}t$ will be included in Eq.(5).[15] In this paper, we focus on the stability margin extrapolation with simulated configurations. Non-linear terms are not introduced as disturbances into the calculation. Moreover, the evolution of the growth rate obtained by using the linear model fits the experimental results several milliseconds after vertical displacement event (VDE) happens,[16] i.e. this approach is suited to the control design and can provide an understandable picture in the vertical stability. A comparison between model prediction and experimental result is shown in Fig.7. Note that all points are taken from different discharges (I_P = 200 kA), with the feedback control set to be zero. The linear model appears to be able to predict the growth rate of vertical instability correctly.

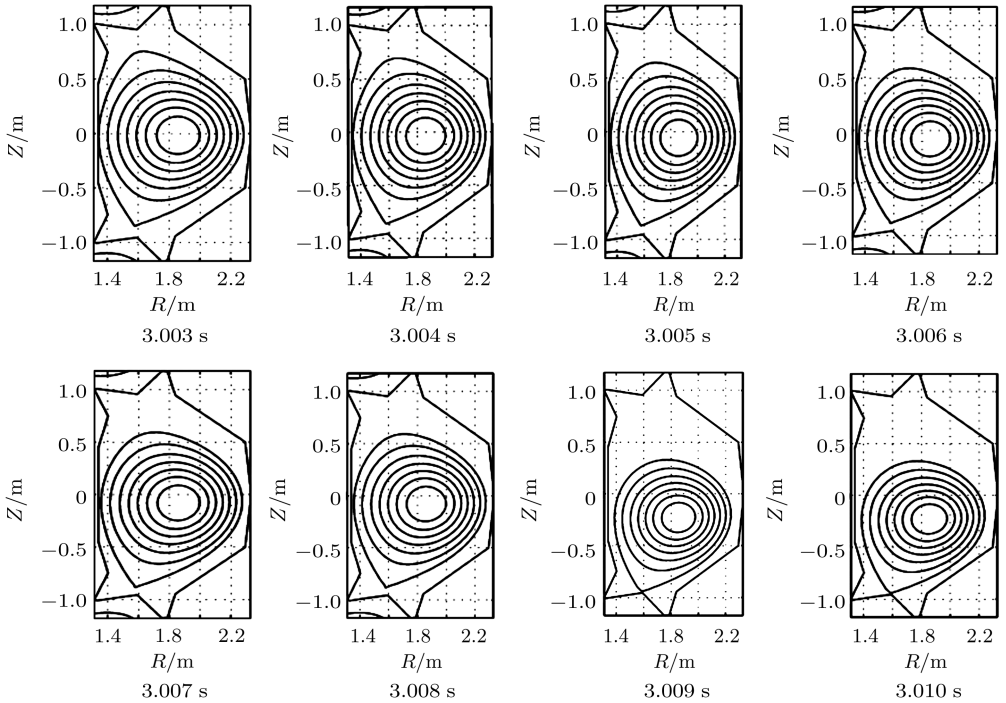


Fig.6. Loss of vertical position control with a feedback cut at 3.0 s for EAST discharge No. 4619.

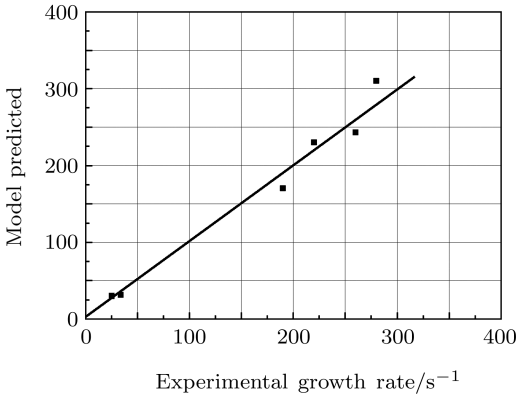


Fig.7. VDE model predicted vs. experimental growth rate with the feedback cut to zero.

4. Extrapolating stability margin with simulation results

What determines the growth rate is the proximity of the plasma current distribution to the passive structure. A larger fraction of the current closer to the structures may lead to a lower growth rate. This can result from a number of factors, such as, plasma shapes (elongation, triangularity and aspect ratio ($A = R/a$)[17,18]) and profiles (internal inductance and poloidal beta). In this section, we will investigate the influence of all parameters mentioned above on growth rate. Note that triangularity δ is fixed to be 0.5 during the simulation, since the EAST is a D-shaped device with a small range for δ.

4.1. Plasma equilibria

In an axisymmetric toroidal system, the MHD equilibrium Grad–Shafranov equation can be written as

$$\Delta^* \psi = -\mu_0 R J_\phi$$

and

$$J_\phi = RP'\,(\psi) + \frac{\mu_0\, FF'\,(\psi)}{4\,\pi^2\, R}. \tag{6}$$

Here, ψ is the poloidal magnetic flux per radian of the toroidal angle ϕ enclosed by a magnetic surface, $F = 2\pi R B_\phi/\mu_0$ and B_ϕ are the poloidal current function and the toroidal magnetic field, and $\Delta^* = R^2\nabla \cdot \left(\nabla/R^2\right)$. The pressure gradient P' and the poloidal current FF' are defined as polynomials,

$$P'(\psi) = \sum \alpha_n y_n(x) \tag{7}$$

and

$$FF'(\psi) = \sum \gamma_n y_n(x), \tag{8}$$

where $x = (\psi - \psi_0)/(\psi_1 - \psi_0)$ is the normalized poloidal magnetic flux, ψ_0 and ψ_1 are the poloidal magnetic flux on the magnetic axis and at the plasma boundary, and $0 \le x \le 1$.

The parameters α_n and γ_n determining the plasma profile were well documented in Ref.[19]. Here we repeat the salient points in that reference. The magnitude of the pressure gradient is changed by varying α_0, and the ratio γ_1/γ_2 determines internal inductance.

4.2. Simulation results

As mentioned earlier,[20] β_p collapse in a highly elongated plasma discharge may cause a vertical disruption. Firstly, the influence of β_p on this instability is investigated by numerical calculation. The value of β_p is scanned by varying the parameter α_0 in Eq.(7). The vertical growth rate with respect to poloidal beta, calculated by using the model mentioned above, is obtained at $l_i = 0.95$, $\delta = 0.5$, $k = 1.9$ and $I_p = 1$ MA, and it is displayed in Fig.8. As shown in the figure, the growth-rate drops monotonically with the value of β_p increasing. The corresponding variation of the current-density profile is plotted in Fig.9. The current density located on the outer-side increases as the value of β_p goes up from low to high. Plasma current distribution is closer to the outer structure, that is to say, low-β_p equilibria are unstabler to the vertical instability for these fixed plasma shape and internal inductance.

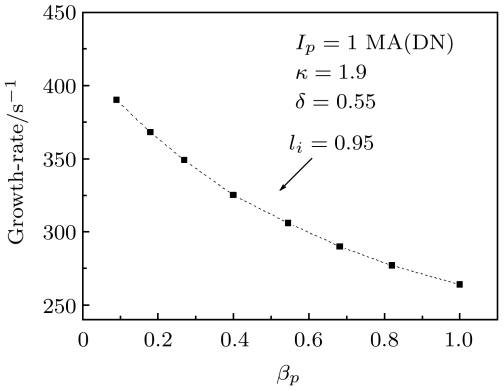


Fig.8. Vertical growth-rate as α function of β_p with $l_i = 0.95 \pm 0.1$.

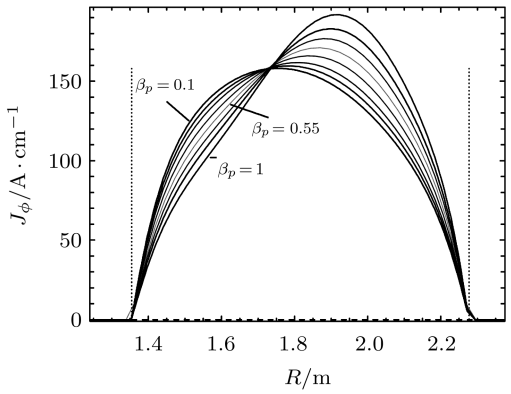


Fig.9. Current density profile versus R, where the curves correspond to β_p over a range from 0.1 to 1.0.

Then we study, for comparison, the vertical instability as a function of l_i by varying the ratio of γ_1/γ_2, separately, at three values of β_p, i.e. 0.1, 0.4 and 0.8, with plasma parameters $I_p = 1$ MA and $\delta = 0.5$. All these results are summarized in Figs.10 and 11.

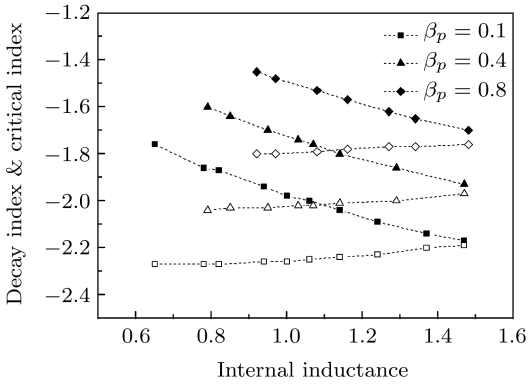


Fig.10. Decay index n and critical index $(-n_c)$ plotted against internal inductance l_i, where curves with solid symbols represent decay index and curves with open symbols refer to critical index.

Figure 10 presents the decay index n and critical index n_c as a function of l_i separately. As is shown, both n and n_c increase with β_p increasing. It is interesting to see that the n_c curves are relatively weakly sensitive to l_i but quite sensitive to β_p. This is probably because the ploidal beta has a stronger effect on Γ than the internal inductance. In Fig.11, the stability margin m_s ($m_s = n_c/n - 1$) and the growth-rate are presented against l_i separately. Results are shown for three different values of β_p, i.e. 0.1, 0.4 and 0.8. The stability margin indicates that some of these cases in simulation will be ended due to VDEs with high growth rates.

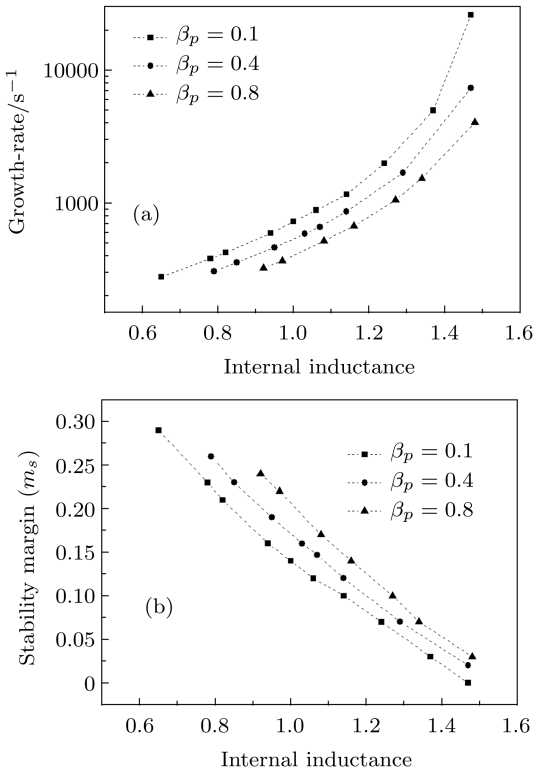


Fig.11. Growth-rate (a) and stability margin (b) versus internal inductance l_i with $A = 3.95 \pm 0.02$.

Finally, the effects of the elongation and the aspect ratio on vertical stability are investigated with $\beta_p = 0.4$, $\delta = 0.5$ (for typical Ohmic discharges of EAST) and l_i varying from 0.8 to 1.5. The cases where elongation values are 1.68, 1.75 and 1.90 and the aspect ratios are 3.95 and 4.19 are investigated separately. An example of plasma boundary for the simulation with $A = 3.95$ is shown in Fig.12. With $A = 4.19$, major and minor radii varied, the obtained results are similar to those shown in Fig.12 and not presented here. The stability margin $M_s(\kappa, l_i, A)$ and the growth rate $\gamma(\kappa, l_i, A)$ versus l_i at different values of aspect ratio and elongation are plotted in Figs.13(a) and 13(b) respectively. We note that the maximum stability margin drops rapidly with elongation degree increasing. The minimum stability margin, corresponding to the ideal $n = 0$ stability limit, is theoretically given by $M_s = 0$. However, in practice, the margin magnitude must be a small positive number. The minimum stability margin will be reported with the plasma that is not sufficiently disrupted, after several campaigns. It is reported that DIII-D and TCV have operated at $M_s = 0.02$ and $M_s = 0.03$ respectively, while large tokamak, like JET, operates at much higher stability margin, specifically $M_s > 0.3$.[21]

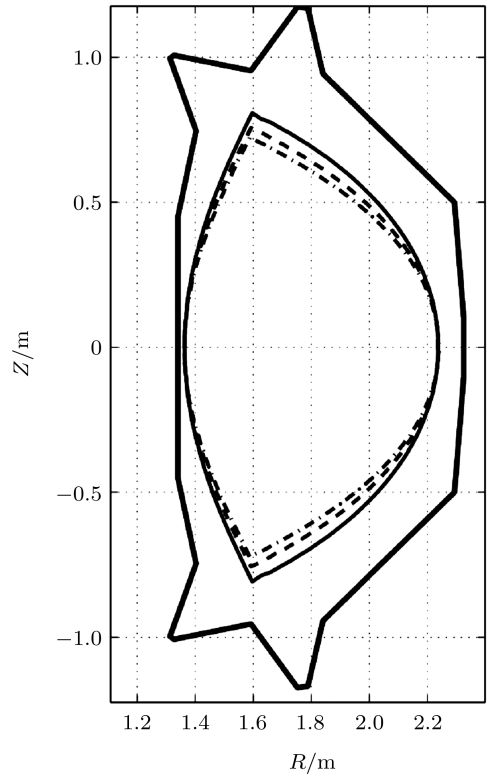


Fig.12. Outline of the fixed boundary in simulation with $A = 3.95$.

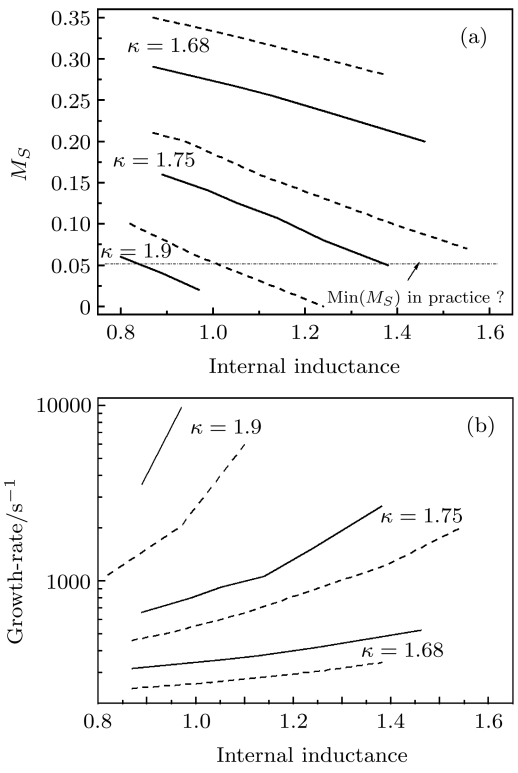


Fig.13. Stability margin (a) and growth-rate (b) versus internal inductance l_i with $\beta_p = 0.4$, $A = 4.19 \pm 0.01$ (solid curves), and $A = 3.95 \pm 0.02$ (dashed curves).

5. Summary and Discussion

We have demonstrated that low-β_p equilibria are more unstable than the vertical instability for a fixed plasma shape and $l_i = 0.95$ (see Fig.8). This is because the radial force F_R moves the current centroid (Shafranov shift) outward gradually due to the value of β_p increasing. One might conclude that increasing β_p could modify the current density, thus benefiting the stabilization of VDEs. However, in this way the passive stabilization will be weakened due to the decreased critical decay index as shown in Fig.10. At $l_i \approx 1.0$, a rough calculation shows that when the values of β_p are 0.1 (case I), 0.4 (case II) and 0.8 (case III), the growth rates are about 750 1/s for case I, 40% less than case I for case II, and 80% less than case I for case III. In the same circumstances, the critical decay indexes are about 2.26 for case I, 12% less than case I for case II, about 25% less than case I for case III. The stability margin magnitudes for cases II and III improve only by 0.02 and 0.04 compared with that of case I by increasing polodial beta. To further investigate l_i, we choose case II as displayed in Fig.11(b). The stability margin magnitude improves by 0.07 as l_i decreases from 1.0 to 0.8. We conclude that for a higher stability margin magnitude, plasma with a lower l_i is stabler than that with a higher β_p for the EAST device.

As expected, in Fig.13(a), solid curves that represent stability margin magnitudes for $A = 4.19$ lie below dashed curves that denote those for $A = 3.95$. This scenario accords with that described in Ref.[11]. Furthermore, all the curves are approximately parallel to each other. The values of ΔM_s, owing to the aspect ratio dropping from 4.19 to 3.95, are almost a constant (0.04) at $\kappa = 1.68$, 1.75 and 1.90. Only changing aspect ratio ($3.8 < A < 4.3$) is insufficient to avoid big disruption of VDE's for elongations of up to 1.90.

In summary, it is clear that lowering the values of elongation and internal inductance is a more effective way to increase the stability margin magnitude than other ways (say, changing the values of A and β_p) in the EAST. We believe that the results in Fig.13 can serve as a good guidance to the choosing of k, l_i and other parameters for the vertical stabilization control. We emphasize here again that the EAST poloidal field coils are relatively far from the plasma. So we have to keep the plasma at a lower vertical instability growth-rate level, or have to mount passive plates inside the

vessel to further extend the stability margin. In future, the stability margin of controllable plasmas toward the ideal instability limit can be investigated under lower plasma current to alleviate the operation risk of the superconducting magnets and thermal shield due to VDEs.

References

[1] Lazarus E A, Lister J B and Neilson G H 1990 *Nucl. Fusion* **30** 111

[2] Jensen T H and Chu M S 1989 *Phys. Fluids* B **1** 1545

[3] Perrone M R and Wesson J A 1981 *Nucl. Fusion* **21** 871

[4] Lister J B, Lazarus E A, Kellman A G, Moret J M, Ferron J R, Helton R J, Lao L L, Leuer J A, Strait E J, Taylor T S and Turnbull A D 1990 *Nucl. Fusion* **30** 2349

[5] Lazarus E A, Chu M S, Ferron J R, Helton F J, Hogan J T, Kellman A G, Lao L L, Lister J B, Strait E J, Taylor T S and Turnbull A D 1991 *Phys. Fluids* B **3** 2220

[6] Wan B N 2007 *Plasma Sci. Technol.* **9** 125

[7] Wan Y X, Weng P D, Li J G, Gao D M, Wu S T and East Team 2000 *20th IAEA Fusion Energy Conference*

[8] Lao L L, St John H and Stambaugh R D 1985 *Nucl. Fusion* **25** 1611

[9] Coutlis A, Bandyopadhyayb I, Lister J B, Vyas P, Albanesec R, Limebeera D J N, Villoned F and Wainwrighta J P 1999 *Nucl. Fusion* **39** 663

[10] Alfredo P 2005 *Nucl. Fusion* **45** 926

[11] Lister J B, Martin Y and Moret J M 1996 *Nucl. Fusion* **36** 1547

[12] Humphreys D A and Yoshino R 1992 *JAERI-M* **92** 069

[13] Humphreys D A private communication

[14] Walker M L and Humphreys D A 2006 *Fusion Science and Technology* **50** 473

[15] Sharma A S [PhD thesis] 2002 Imperical College of Science, Technology and Medicine (London: United Kingdom)

[16] Qian J P, Wan B N, Shen B, Xiao B J, Sun Y W, Shi Y J, Lin S Y, Li J G and Gong X Z 2008 *Plasma Sci. Technol.* **10** 290

[17] Hofmann F, Moret J M and Ward D J 1998 *Nucl. Fusion* **38** 1767

[18] Stambaugh R D, Lao L L and Lazarus E A 1992 *Nucl. Fusion* **32** 1642

[19] Howl W, Turnbull A D, Taylor T S, Lao L L, Helton F J, Ferron J R and Strait E J 1992 *Phys. Fluids* B **4** 1724

[20] Makamura Y, Lister J B, Hofmann F, Martin Y R, Moret J M and Vyas P 1999 *26th EPS Conf. on Contr. Fusion and Plasma Physics* Vol **23** J 417

[21] Hofmann F, Coda S, Lavanchy P, Llobet X, Marmillod P, Martin Y, Martynov A, Mlynar J, Moret J M, Pochelon A and Sauter O 2002 *Nucl. Fusion* **42** 743